

Evidence That NiNi Acetyl-CoA Synthase Is Active and That the CuNi Enzyme Is Not[†]

Javier Seravalli,[‡] Yuming Xiao,[§] Weiwei Gu,[§] Stephen P. Cramer,[§] William E. Antholine,^{||} Vladimir Krymov,^{⊥, #} Gary J. Gerfen,[⊥] and Stephen W. Ragsdale^{*:‡}

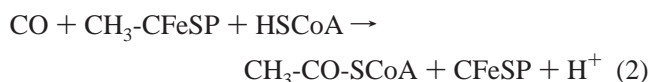
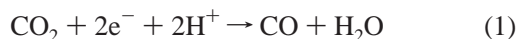
Department of Biochemistry, University of Nebraska—Lincoln, Lincoln, Nebraska 68588-0664, Department of Applied Science, University of California, Davis, California 95616, National Biomedical ESR Center, Medical College of Wisconsin, Milwaukee, Wisconsin 53226-0509, Department of Physiology and Biophysics, Albert Einstein College of Medicine of Yeshiva University, Bronx, New York 10461, and Donetsk Physical-Technical Institute, Ukrainian National Academy of Sciences, Donetsk, Ukraine

Received December 6, 2003; Revised Manuscript Received January 30, 2004

ABSTRACT: The bifunctional CO dehydrogenase/acetyl-CoA synthase (CODH/ACS) plays a central role in the Wood–Ljungdahl pathway of autotrophic CO₂ fixation. One structure of the *Moorella thermoacetica* enzyme revealed that the active site of ACS (the A-cluster) consists of a [4Fe-4S] cluster bridged to a binuclear CuNi center with Cu at the proximal metal site (M_p) and Ni at the distal metal site (M_d). In another structure of the same enzyme, Ni or Zn was present at M_p. On the basis of a positive correlation between ACS activity and Cu content, we had proposed that the Cu-containing enzyme is active [Seravalli, J., et al. (2003) *Proc. Natl. Acad. Sci. U.S.A.* 100, 3689–3694]. Here we have reexamined this proposal. Enzyme preparations with a wider range of Ni (1.6–2.8) and Cu (0.2–1.1) stoichiometries per dimer were studied to reexamine the correlation, if any, between the Ni and Cu content and ACS activity. In addition, the effects of *o*-phenanthroline (which removes Ni but not Cu) and neocuproine (which removes Cu but not Ni) on ACS activity were determined. EXAFS results indicate that these chelators selectively remove M_p. Multifrequency EPR spectra (3–130 GHz) of the paramagnetic NiFeC state of the A-cluster were examined to investigate the electronic state of this proposed intermediate in the ACS reaction mechanism. The combined results strongly indicate that the CuNi enzyme is inactive, that the NiNi enzyme is active, and that the NiNi enzyme is responsible for the NiFeC EPR signal. The results also support an electronic structure of the NiFeC-eliciting species as a [4Fe-4S]²⁺ (net *S* = 0) cluster bridged to a Ni¹⁺ (*S* = 1/2) at M_p that is bridged to planar four-coordinate Ni²⁺ (*S* = 0) at M_d, with the spin predominantly on the Ni¹⁺. Furthermore, these studies suggest that M_p is inserted during cell growth. The apparent vulnerability of the proximal metal site in the A-cluster to substitution with different metals appears to underlie the heterogeneity observed in samples that has confounded studies of CODH/ACS for many years. On the basis of this principle, a protocol to generate nearly homogeneous preparations of the active NiNi form of ACS was achieved with NiFeC signals of ~0.8 spin/mol.

The bifunctional enzyme CODH/ACS¹ plays a central role in the Wood–Ljungdahl pathway of autotrophic CO₂ fixation (1, 2). The small β subunit of this enzyme complex (CODH, AcsA) catalyzes the two-electron reduction of CO₂ to CO (eq 1), which migrates through a 140 Å channel from the CODH active site (cluster C) to the A-cluster, which is the

active site of the α subunit (ACS, AcsB). Here, the CO condenses with a methyl group (donated by the methylated corrinoid iron–sulfur protein, CH₃-CFeSP) and CoA to generate acetyl-CoA (eq 2) (3).



Two recent crystal structures reveal that CODH/ACS is a 300 kDa α₂β₂ protein with two core CODH β subunits tethered on each side to two ACS α subunits (4, 5). In both structures, the β subunit contains 1 Ni and 10 Fe ions (per monomeric unit) arranged into three FeS clusters, known as B, C, and D, while the α subunit contains the A-cluster, which is a [Fe₄S₄]^{2+/1+} cubane that is bridged by a cysteinyl sulfur (Cys⁵⁰⁹) to the proximal metal of a binuclear center. Additionally, both structures reveal that the binuclear center

[†] This research was supported by NIH Grant GM39451 (S.W.R.), NIH Grant RR01008 (W.E.A.), NSF Grant DBI 0096713 (G.J.G.), and NIH Grant GM60609 (G.J.G.).

* To whom correspondence should be addressed: (402) 472-2943 (phone); (402) 472-7842 (fax); sragdale1@unl.edu (e-mail).

[‡] University of Nebraska—Lincoln.

[§] University of California, Davis.

^{||} Medical College of Wisconsin.

[⊥] Albert Einstein College of Medicine of Yeshiva University.

[#] Ukrainian National Academy of Sciences.

¹ Abbreviations: CODH, carbon monoxide dehydrogenase; ACS, acetyl-CoA synthase; IR, infrared; FTIR, Fourier transform infrared; EDTA, ethylenediaminetetraacetic acid; Tris, 2-amino-2-(hydroxymethyl)-1,3-propanediol; DTT, dithiothreitol; ophen, *o*-phenanthroline; EPR, electron paramagnetic resonance; neo, neocuproine; HFEDPR, high-frequency echo-detected (pulsed) EPR.

contains a square planar nickel ion (the distal Ni, Ni_d) coordinated in an N₂S₂ ligand environment by the side-chain sulfur atoms of Cys⁵⁹⁵ and Cys⁵⁹⁷ and by two backbone nitrogen atoms of Gly⁵⁹⁶ and Cys⁵⁹⁷. The two structures differ in the metal composition of the proximal metal (M_p) that bridges the cluster and the distal Ni. In one case, this metal is a distorted tetrahedral Cu ligated by three sulfurs of Cys⁵⁰⁹, Cys⁵⁹⁵, and Cys⁵⁹⁷ and a nonprotein ligand (4). In the other structure, two α subunits are in different conformations, each containing a different M_p (5). One α subunit is in a "closed" conformation and contains a distorted tetrahedral Zn ion at M_p, while the other α subunit, which is in an "open" conformation, contains a square planar Ni coordinated by the three μ^2 -bridging cysteine thiolates just mentioned (Cys⁵⁰⁹, Cys⁵⁹⁵, and Cys⁵⁹⁷) and an unidentified exogenous ligand (5). Thus, in one structure a CuNi binuclear center is present in both ACS subunits; in the other structure, there is a NiNi center in one ACS subunit and ZnNi in the other.

In a recent paper, we concluded that the CuNi form of ACS is active (6). This was based on a positive correlation between the amount of Cu and ACS activity in preparations of CODH/ACS that had between 1.9 and 2.3 mol of Ni/mol of enzyme and similar high levels of CODH activity. Our analysis was based on the assumption that only the composition of the proximal metal site would vary in these preparations while the distal site would be saturated with nickel. Four recent papers (5, 7–9) raise several questions about the proposal that Cu is a component of active ACS (6). First, Cu has not been observed in spectroscopic studies of the protein. However, among the various spectroscopic methods utilized (EPR, ENDOR, Mössbauer, UV–visible, XAS), only XAS studies would have revealed Cu¹⁺ and, even in this case, only when the beam was focused on the Cu absorption edge. When EXAFS and XANES were performed on CODH/ACS, Cu¹⁺ was detected with the expected Cu–Ni distance (6). A second issue is the demonstration that removal of Ni by *o*-phenanthroline (ophen) results in loss of ACS activity and readdition of Ni restores activity (10, 11); however, since the presence of Cu in CODH/ACS was unknown at that time, the effect of Cu addition was not addressed. A recent report showed that adding Ni to metal-depleted samples of CODH/ACS restores acetyl-CoA synthase activity, the ability to transfer methyl groups, and NiFeC EPR signal intensity, whereas addition of Cu²⁺ does not (9). These results indeed suggest that the NiNi form of ACS is active and the CuNi is not; however, Cu²⁺ treatment led to a protein with 11 mol of Cu/mol of enzyme, and results described here show that Cu²⁺ damages both CODH and ACS activity. A third issue is that the recombinant *Methanosarcina thermophila* ACS subunit could be reconstituted actively with Ni but not Cu; however, only NiNi and CuCu forms of the enzyme were generated, not the relevant CuNi enzyme (8). A fourth concern is that the Cu enzyme was stated to be inconsistent with the required electron count. However, acetyl-CoA synthesis from the methylated corrinoid FeS protein, CO, and CoA does not involve net redox chemistry, and the proposed internal redox reactions during catalysis could be explained by several alternative mechanisms, since [Fe₄S₄] clusters can exist in two oxidation states (2+ and +1), Cu as 1+ or 2+, and Ni in the 1+, 2+, or 3+ states. Thus, unequivocal conclusions about the catalytic proficiency of

the NiNi versus CuNi forms of ACS cannot be made on the basis of the published literature.

Of the various issues discussed above, the second raises the most serious questions about the activity of the CuNi form of the enzyme. Here, we describe the analysis of several more preparations of CODH/ACS that have a wider range of Ni (1.6–2.8) and Cu (0.2–1.1) stoichiometries per dimer, allowing us to reexamine the correlation between the Ni and Cu content and ACS activity. This has led us to question the validity of the assumption (i.e., of focusing on samples with 2.0 mol of Ni/mol) that we made in the previous analysis. To further address the relevance of the NiNi and CuNi enzymes, we determined the effect of ophen, which removes Ni but not Cu, and neocuproine (neo), which removes Cu but not Ni, on ACS activity (CO exchange, CoA exchange, acetyl-CoA synthesis, and NiFeC signal intensity) in the purified enzyme and in cell extracts. We also addressed whether these chelators remove the metal from the M_p or the M_d site. By collecting EPR spectra at multiple frequencies (3–130 GHz), we addressed the electronic state of the paramagnetic NiFeC species and whether the NiFeC EPR signal arises from the NiNi or the CuNi form of the enzyme. Finally, we assessed whether Cu is introduced into the M_p site during cell growth or during enzyme purification and tested the hypothesis that, by controlling the metal composition of the A-cluster, homogeneously active preparations of ACS can be prepared.

MATERIALS AND METHODS

Materials. CO (99.98%) and N₂ (99.998%) were purchased from Linweld (Lincoln, NE), and other inert gases were freed from traces of oxygen by passage over a heated BASF catalyst. All other chemicals were from Aldrich, Sigma, or Becton Dickinson (Sparks, MD) and were of the highest purity available.

Purification and Manipulation of CODH/ACS. *Moorella thermoacetica* (formerly *Clostridium thermoaceticum* strain ATCC 39073) was grown with 0.1 M glucose as the carbon source at 55 °C in undefined (12) media. All glassware and fermentation equipment were washed with dilute hydrochloric acid followed by Nanopure water prior to use. The Nanopure water was found to contain the following elements: Ca (1.51 ppb), Cu (0.244 ppb), Fe (0.068 ppb), Mg (1.55 ppb), Mo (0.049 ppb), Ni (0.021 ppb), and Zn (0.185 ppb). CODH/ACS was purified under strictly anaerobic conditions (13) in a Vacuum Atmospheres (Hawthorne, CA) glovebox maintained at 18 °C at an oxygen tension below 1 ppm. Oxygen levels were monitored continuously with a Model 317-trace oxygen analyzer (Teledyne Analytical Instruments, City of Industry, CA). CODH/ACS was >95% pure on the basis of denaturing SDS–PAGE electrophoresis.

For metal analysis of *M. thermoacetica* cells, cultures were grown in 1 L bottles with 0.1 M glucose and saturating CO₂ as carbon sources (12). Cells were harvested anaerobically using acid-washed JA20 bottles from Beckman. The cells were washed three times with 50 mM Tris-HCl, pH = 7.6, containing 2 mM DTT, 2 mM sodium dithionite, and 0.1 mM methyl viologen, followed by centrifugation at 10000 rpm for 5 min. The wet cell paste was then lyophilized in order to obtain a cell dry weight. After constant dry weight was reached (1 day), the cell powder was suspended

anaerobically in lysis buffer, consisting of wash buffer supplemented with 0.25 mg/mL lysozyme, 2 units/mL deoxyribonuclease I, and 0.2 mM PMSF. The metal concentrations of the lysis buffer were used as a blank for subtraction from the sample concentrations.

CODH activity was measured at 55 °C, 50 mM Tris-HCl, pH 7.6, and 2 mM DTT with 10 mM methyl viologen as electron acceptor (13). The isotopic exchange reaction between CO and [1-¹⁴C]acetyl-CoA was measured at 55 °C using 200 μM acetyl-CoA, 0.57 mM CO, 0.1 M MES, pH 6.0, and 0.1 mM methyl viologen. Reactions were started by addition of 0.05 μCi of [1-¹⁴C]acetyl-CoA. Acetyl group exchange assays were performed as described (14) with 0.1 mM each of acetyl-CoA and 3'-dephospho-CoA in the presence of 1.0 mM titanium citrate. The 0.1 M HCl quenched samples were analyzed by HPLC with a μ-Bondapak C₁₈ analytical column (Waters Corp., Milford, MA) using an isocratic elution method with 15% methanol in 50 mM potassium phosphate, pH 5.60. The concentration of 3'-dephospho-CoA was determined from integration of the corresponding peak area. Acetyl-CoA synthesis was monitored by UV-visible spectroscopy at 55 °C, 1 atm of CO, 0.5 mM coenzyme A, and 20 μM CH₃-CFeSP as previously described (15), and acetyl-CoA formation was confirmed by HPLC analysis. Because of the acute inhibition by CO (16), acetyl-CoA synthesis activities under these conditions measured with 1 atm of CO are 7% as high as those determined with 10% CO, so one can multiply these activities by 14.3 to obtain the "maximal" values.

Protein concentrations were determined by the Rose Bengal method (17). Metal analysis was performed at the Chemical Analysis Laboratory at the University of Georgia (Athens, GA) using inductively coupled argon plasma (ICP) detection for 20 elements, which includes Ni, Cu, Zn, and Fe.

Western analysis was performed on 12.5% SDS-PAGE denaturing gels. Samples of highly purified (>95% purity) CODH/ACS (12, 0.25, 0.5, 1.0, 2.0, and 4.5 μg) were loaded in separate lanes to serve as standards. Then, samples (5–20 μg of total protein) of the pooled fractions from the cell-free extract and from the DEAE, Q-Sepharose, and phenyl-Sepharose columns were loaded in separate lanes. Total protein concentrations were estimated using the Rose Bengal assay (17). After electrophoresis and electroblotting the SDS-PAGE gel onto a nitrocellulose membrane, the membrane was blocked with 2.5% gelatin in TBS buffer (20 mM Tris-HCl, pH = 7.50, 0.5 M NaCl) for 20 min, washed twice with TTBS buffer (TBS buffer supplemented with 0.5% v/v Tween 20), incubated with purified rabbit anti-CODH/ACS polyclonal antibodies in TTBS, and washed twice with TTBS buffer. The membrane was then incubated with a 1/5000 dilution of goat anti-rabbit alkaline phosphatase antibody conjugate (Sigma Chemical Co., St. Louis, MO) in TTBS, washed with TTBS and TBS buffers, and stained with BCIP (5-bromo-4-chloro-3-indolyl phosphate, 0.3 mg/mL) (Amresco, Solon, OH) and NBT (nitro blue tetrazolium, 0.15 mg/mL) (Sigma Chemical Co.). The areas and intensities for the bands corresponding to CODH (72 kDa) and ACS (82 kDa) were estimated using a Bio-Rad Chemi-Doc densitometer equipped with the software package Quantity One (Bio-Rad, Hercules, CA). By inclusion of the CODH/ACS standards, immunological determination of CODH/ACS

amounts agrees very well with values determined by CODH activity assays. Furthermore, the calibration curve with purified CODH/ACS as standard (not shown) is linear within the range of CODH/ACS amounts used in the analysis.

Metal Removal. Metal chelators, ophen and neo, were dissolved in 0.1 M Tris-HCl, pH 7.60, at concentrations of 0.3 and 0.15 mM, respectively. For the treatment of *M. thermoacetica* cell extracts, 2 mL of cell extract with protein concentrations between 15 and 20 mg mL⁻¹ was mixed with 6 mL of either the chelator solution or a control buffer solution. After overnight incubation, the samples were concentrated and diluted 300-fold, finally to 2 mL, using a Diaflo membrane with a size exclusion limit of 30000 Da. The resulting samples were then split into 2–1.0 mL fractions, one of which was treated with 2.0 mM NiCl₂ and the other served as control. Activities and EPR spectra were obtained for these samples after overnight incubation. For purified CODH/ACS, 30 equiv of neocuproine or 10 equiv of *o*-phenanthroline was added to the protein after buffer exchange into 0.1 M Tris-HCl, pH 7.60, without reductants. After ~2 h incubation time at 55 °C the samples were monitored for the loss of the NiFeC signal by EPR spectroscopy to assess loss of Ni from ACS. After removal of unbound metal ions and low molecular weight complexes by repeated dilution and concentration using an Amicon concentration with a YM30 membrane, metal reconstitution was carried out by addition of 2 equiv of either NiCl₂ in 0.1 M Tris-HCl, pH 7.60, or CuCl in HCl neutralized with 50 mM CAPSO, pH 10.0. Unbound added metals were removed by diafiltration.

EPR and XAS Spectroscopy. Routinely, X-band EPR spectra were recorded in a Bruker ESP300e spectrometer connected to a Hewlett-Packard microwave frequency counter, model 5253B, and a Bruker gaussmeter, model ER 035. Samples were exposed to 1 atm of CO for 10–15 min to allow formation of the NiFeC signal and frozen in liquid nitrogen.

For multifrequency EPR, four spectrometers were employed. Between 3 and 35 GHz, Varian E109 and E-9 systems operating at ~9.1 GHz (X-band) and ~35.1 GHz (Q-band), respectively, and a low-frequency (S-band) system based on the loop-gap resonator designed by Froncisz and Hyde (18) at the National Biomedical ESR Center, Medical College of Wisconsin, were used. The Q-band bridge was modified with addition of a GaAs field-effect transistor signal amplifier and low-noise Gunn diode oscillator (19). At Q-band, the parameters were as follows: microwave frequency, 35.0 GHz; power, 10 dB; modulation amplitude, 10 G; gain, 400; temperature, -140 °C; seven scans averaged. The X-band spectra were collected using a Varian E-9 ESR spectrometer with the following instrumental parameters: microwave frequency, 9.04 GHz; power, 5 mW; modulation amplitude, 5 G; gain, 8000; temperature, -140 °C. The S-band system consists of a Varian E-9 ESR spectrometer fitted with a low-frequency microwave bridge operating at 3.4 GHz (S-band). The instrument parameters for the S-band spectra were as follows: microwave frequency, 3.33 GHz; power, 16 dB (10 mW); modulation amplitude, 5 G; gain, 250; temperature, -140 °C; four scans averaged. Measurements at different frequencies were carried out at -140 °C (Figure 2) and 10–15 K (data not shown). Microwave frequencies were measured with an EIP model 331 counter,

and the magnetic field was calibrated with an MJ-110R Radiopan NMR magnetometer at S- and X-band. The range of the field at Q-band was determined from Mn lines.

High-frequency echo-detected (pulsed) EPR (HFDEPR) spectra at 130 GHz (D-band) were collected at 10 K using a spectrometer previously described (20) with the following modifications. To facilitate field calibration and to maximize sensitivity, the echo-detected spectra were acquired with 10 G, 300 Hz square wave field modulation, yielding the derivative presentation directly from the spectrometer. Two data channels acquired in quadrature were used to generate the correctly phased absorption spectrum. The magnetic field was calibrated using proton HFENDOR performed directly on the NiFeC sample. This method yielded an uncertainty in the field measurement of ~ 8 G, which translates to an uncertainty in the g -value of ~ 0.0004 . A two-pulse HFDEPR sequence was used with pulse widths of 50 ns and delay between the pulses of 150 ns. The spectra are an average of four scans of 300 shots per point. The instrument settings for the D-band spectra were as follows: temperature, 10 K; microwave frequency, 130.010 GHz; power ~ 70 mW at output of bridge; repetition rate, 300 Hz; square wave field modulation, 150 Hz; modulation amplitude, 10 G; pulse widths of Hahn echo sequence, 50 ns; time between pulses, 150 ns; average of four scans of 300 shots per point.

XAS experiments were performed at the Biophysics Collaborative Access Team (BioCAT) beamline at the Advanced Photon Source (APS) using a Si double-crystal monochromator with a (1,1,1) orientation. Higher harmonics were rejected by the focusing mirror. The incident beam was guarded by a 0.5 mm vertical by 1 mm horizontal slit in front of the samples. The maximum incident flux was 10^{13} photons/s at 8000 eV, as monitored by a nitrogen-filled ion chamber placed downstream of the guarding slit. X-ray energies were calibrated by simultaneous measurement of a Cu foil absorption spectrum, assigning the first inflection point as 8980.3 eV. During all X-ray measurements, samples were maintained at 30 K using a He displax cryostat. The data were recorded with dual photomultiplier detectors and a 1 eV point spacing at a constant 25 ms per point over an electronvolt range of 8879–9679 for a total collection time of 20 s per scan. To prevent detector saturation, the incident beam intensity was attenuated by Al foils that were inserted upstream of the guarding slit. XAS data were analyzed as described previously (6). The final spectra were averaged over a total of 230 scans.

RESULTS

Metal Composition—Activity Correlations. It is important to identify the metal at the proximal site (M_p) in the A-cluster of the active form of ACS. Here, we will refer to the enzyme with Cu in the M_p site as the CuNi enzyme and that with Ni in that site as the NiNi enzyme. We have analyzed many enzyme preparations that have a wider range of Ni (1.6–2.8) and Cu (0.2–1.1) stoichiometries than earlier, allowing us to reexamine the dependence of the ACS (Figure 1A) and the CODH activities and NiFeC EPR signal intensity (Figure 1B) on the Ni and Cu contents. The typical NiFeC EPR signal is shown in Figure 2. The data from our previous study are replotted as the open circles joined point by point by a solid line (Figure 1A). These results lead us to question

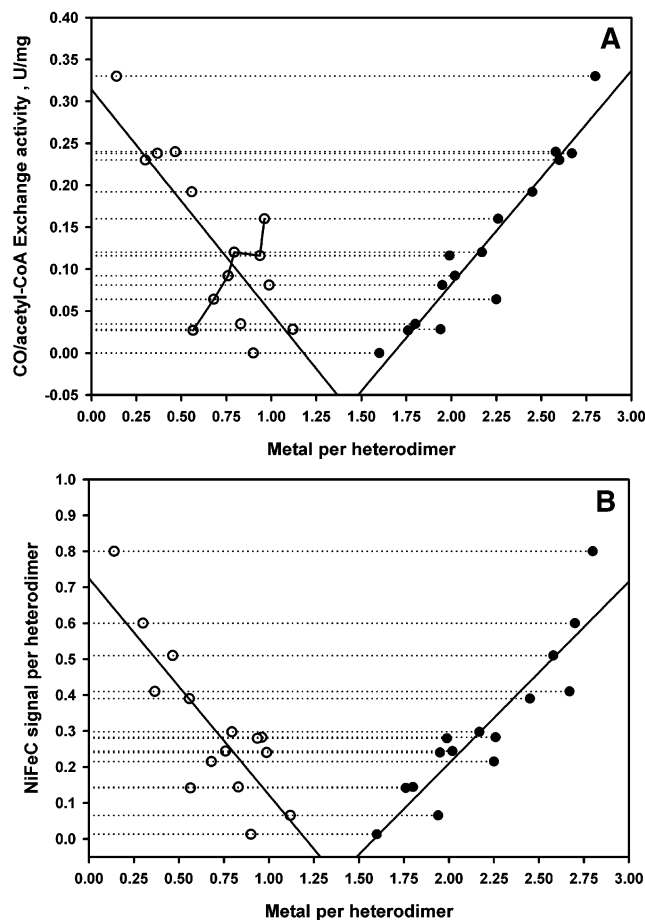


FIGURE 1: Dependence of the acetyl-CoA/CO carbonyl exchange rate (A) and NiFeC EPR signal (B) on the Ni and Cu contents of purified ACS/CODH samples, expressed per heterodimeric unit. Assays and EPR spectroscopy were performed as indicated in Materials and Methods. Open circles are for Cu, and closed circles are for Ni. Cu and Ni contents for a given sample are joined by a dotted line to the y-axis. Solid lines were obtained by nonlinear regression fit of either activity or EPR intensity versus Cu or Ni contents. Previously published Cu data are joined point by point by a solid line. In earlier studies, a negative relationship between Zn and activity was also observed (14).

the validity of the assumption that one should correlate activity only in samples that contain high levels of CODH activity and 2.0 mol of metal/mol of enzyme, which we made in the previous analysis (6) for the following reasons. First, it appears that Ni is labile not only in the A-cluster, since zero activity is associated with a Ni content of 1.6 (not 2.0), indicating that the Ni atom of the C-cluster and/or the distal Ni in the A-cluster is also labile (Figure 1B). Second, there is a strong correlation between ACS activity and Ni content (extending well above 2.0 Ni per heterodimer) with a slope of 0.50 ± 0.06 , indicating that 2 Ni atoms per heterodimer (Figure 1) are required for ACS activity and for NiFeC signal formation. On the other hand, there is a negative correlation with Cu content (Figure 1). The previously observed weak dependence of activity on Cu (open circles joined point by point in Figure 1A) appears to have occurred because these samples also contained slightly higher amounts of Ni, and this weak positive activity/Cu dependence within this subset of data is clearly dwarfed by the strong relationships just described. These results strongly suggest that the NiNi enzyme is active and that the CuNi enzyme is inactive.

Table 1: Chelator Effect on Purified ACS/CODH

	Fe	Ni	Cu	Zn	CODH (units/mg)	ACS (milliunits/mg)	CoASH exchange (units/mg)	NiFeC spins/ heterodimer
as isolated I	13.9	2.6	0.5	<0.1	425	100	1870	0.59
open I	13.5	2.0	0.6	0.50	302	18.3		0.09
open I + Ni ²⁺	12.8	2.6	0.7	0.40	260	44.5	1038	0.21
open I + Cu ¹⁺	13.2	2.0	1.2	1.0	380	17.0	220	0.088
open I + Cu ²⁺	11.5	1.74	2.2		56	1.72	58	~0
as isolated II	14.7	2.83	0.13	0.15	434	148	2550	0.80
open II	15.7	2.08	0.17	0.34	381	6	160	0.035
open II + Ni ²⁺	16	2.87	0.19	0.60	420	122	1120	0.59
open II + Cu ¹⁺	15.5	2.18	1.50	0.50	380	12	30	0.036
open II + Ni ²⁺ + Cu ¹⁺	13.7	3.4	1.5	1.6	330	96	660	0.47
open II + Cu ¹⁺ + Ni ²⁺	12.9	2.15	0.41	>2.0	350	21	31	<0.02
as isolated III	14.3	2.74	0.31	0.16	312	90		0.58
III + neo	14	1.93	0.21	~0	333	85		0.46
III + neo + Ni ²⁺ ^a	14	>3 ^a	0.20	~0	401	149		0.80

^a The Ni measurement was unreliable in this sample.²

Table 2: Chelator Effect on *M. thermoacetica* Cell-Free Extracts

	CO oxidation (units/mg)	acetyl-CoA synthesis (milliunits/ mg) ^a	CoA/ acetyl-CoA exchange (units/mg)	NiFeC (μ M)	NiFeC mg of protein
untreated	12.2	41	75	0.53	0.033
open	11.5	3.5	25	~0	~0
open + Ni ²⁺	14.1	21	56	0.28	0.025
neo + Ni ²⁺	11.6	82	117	1.05	0.082
neo + Cu ¹⁺	6.7	20		0.25	0.031

^a Acetyl-CoA synthesis was assayed with 10% CO and 90% nitrogen balance ([CO] = 57 μ M) at 55 °C.

Metal Chelation Studies. To further address the relevance of the NiNi and CuNi enzymes, we determined the effect of open and neo on ACS activity (CO/acetyl-CoA exchange, CoA/acetyl-CoA exchange, and acetyl-CoA synthesis) and NiFeC signal intensity in purified enzyme (Table 1) and in cell extracts (Table 2). As described earlier, open removes the “labile Ni” from the A-cluster (21), and neo is a potent Cu¹⁺ chelator. Both chelators are relatively specific in that open does not affect the Cu content and neo does not affect the Ni content (Table 1). The Zn content varies among different preparations, and neither open nor neo have a consistent effect on the Zn content. As observed earlier (14), a high Zn level is correlated with low ACS activity; however, as shown in Table 1, it is obvious that Zn can occupy sites on CODH/ACS unrelated to the A- or C-clusters. The two CODH/ACS samples described here contained 0.6 and 0.8 spin/mol of NiFeC EPR signal, and treatment with open removes 0.6 and 0.8 Ni, respectively, and leads to nearly complete loss of the NiFeC signal and ACS activity of the pure enzyme. Addition of Ni increases the Ni content to 2.6 and 2.8, respectively, and restores 50–70% of the ACS activity and NiFeC signal intensity. However, while addition of Cu¹⁺ to the open-treated enzyme increases the Cu content to 1.0 Cu/mol, this treatment does not increase CODH or ACS activity. Thus, Ni, but not Cu, is able to increase ACS activity of the open-treated cell extract or pure enzyme.

The above results indicate that, when CODH/ACS is treated with open, Ni is incorporated into the metal-depleted proximal site in the A-cluster. Does Cu¹⁺ also bind to this in vitro depleted site or elsewhere in the protein? When Ni²⁺ is added to the (i) open-treated enzyme and then (ii) Cu¹⁺-treated enzyme, activity does not increase, indicating that

open removes Ni²⁺, but not Cu, from the proximal metal site and that Cu¹⁺ can occupy the proximal site but does not support activity. That Ni does not restore activity of the Cu¹⁺-treated enzyme indicates that Cu¹⁺ is present at the proximal metal center, which blocks binding of Ni. The location of the reconstituted Cu is further addressed by experiments using neo as a chelator and by X-ray absorption spectroscopic analysis.

XANES analysis of the open- and Cu-treated enzyme clearly indicates that all of the Cu is in the Cu¹⁺ state (data not shown), as observed earlier (6). Cu-EXAFS analysis of the same preparation of enzyme (Figure 3, Table 4) indicates that the Cu environment includes 2.5 S (2.32 Å), 1 Ni (2.78 Å), and 1 N or O (1.95 Å); however, a model including 3 S, 1 N/O, and 1 Ni is also a reasonable fit to the spectrum. The data indicate that all of the Cu ions in the protein have another metal located 2.78 Å away; thus apparently all of the Cu is reconstituted into a site that is near another metal. These results are similar to those described earlier for the native Cu-containing enzyme. Previously, the Cu-EXAFS data of the as isolated enzyme were best fit by a model including 3 S (2.25 Å) and 1 Ni (2.65 Å) (6), while the crystal structure assigned three Cu–S bonds at distances ranging from 2.16 to 2.28 Å, an unknown ligand, and a Cu–Ni bond distance of 2.69 Å. These results provide direct structural evidence supporting the enzymatic studies described above that the reconstituted Cu is located in the M_p site.

When the purified enzyme is treated with open and then Cu²⁺, both CO oxidation and ACS activities decrease (Table 1). Inhibition of ACS activity by Cu²⁺ was earlier cited as evidence that the CuNi enzyme is inactive (9); however, this effect is also observed in the absence of chelator, indicating that Cu²⁺ inactivates the protein by a mechanism that does not (solely) involve occupancy of the proximal metal site. Unlike Cu²⁺, the effect of Cu¹⁺ is specific to ACS and appears to require depletion of the M_p site.

Treatment of the pure enzyme with ~5 equiv of neo does not remove Ni²⁺ since the NiFeC signal intensity does not decrease. Treatment with a higher neo ratio (30-fold) leads to loss of this paramagnetic signal, and adding Ni to this neo-incubated pure enzyme markedly increases ACS activity without affecting the CODH activity (Table 1).² A similar effect is observed with *M. thermoacetica* cell-free extracts.

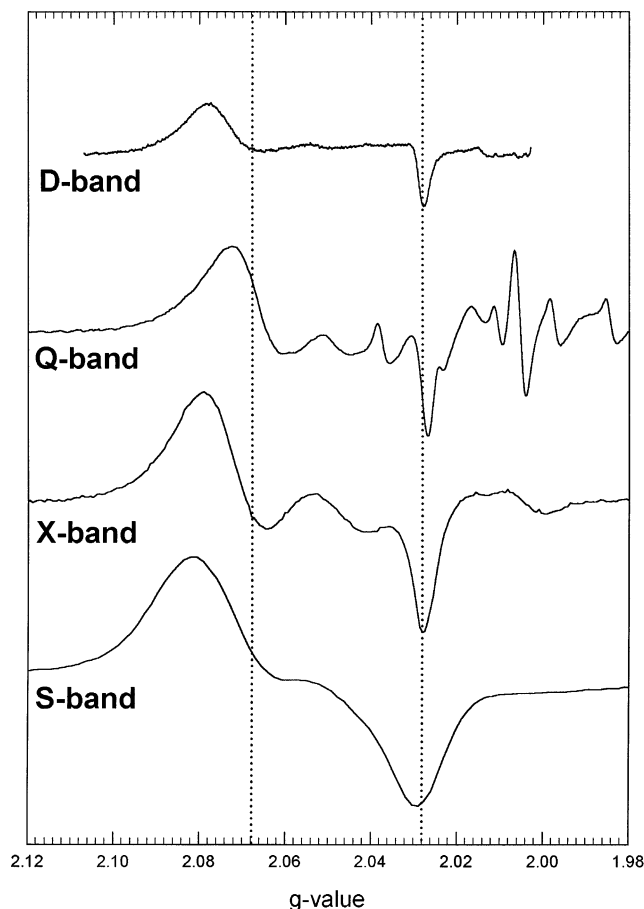


FIGURE 2: Multifrequency EPR studies. Instrument settings are given in Materials and Methods. Extra lines in the Q-band spectrum are Mn lines and a free radical line from the cavity. All spectra show a minor contribution from the $g = 2.055, 2.028$ signal of an altered form of cluster A (23). The line widths in units of magnetic field (and in units of g) of the $g = 2.07$ peak are 12 G (0.021 g-units), 22 G (0.014 g), 71 G (0.013 g), and 253 G (0.021 g) at S-, X-, Q-, and D-bands, respectively. The full widths at half-height in units of field (and g) for the $g = 2.03$ feature are 6.3 G (0.0171 g-units), 9.6 G (0.008 g), 21 G (0.0029 g), and 71 G (0.0038 g) at S-, X-, Q-, and D-bands, respectively.

Addition of Cu^+ or neo does not affect the CODH or ACS activities (Table 2), but if Ni^{2+} is then added to neocuproine-treated cell extracts, both the ACS activity and the NiFeC spin intensity increase without affecting CODH activity. The 4-fold increase in ACS activity would be consistent with replacement of Cu with Ni to generate nearly homogeneous NiNi ACS.

To further test the metal replacement strategy, we prepared a cell-free extract from a large batch of *M. thermoacetica* cells grown in the presence of $4 \mu\text{M}$ CuCl_2 and $20 \mu\text{M}$ NiCl_2 . The major portion of the cell extract was used to purify CODH/ACS, resulting in a protein with 13.6 Fe, 0.4 Cu, and 2.6 Ni per heterodimer, as determined by ICP analysis (labeled "as isolated III" in Table 1). The minor portion was treated with neo first and then with NiCl_2 . A 66% increase in the NiFeC signal and 50% increase in acetyl-CoA synthesis activity were observed in the cell extracts (see

² For sample III (III + Neo + Ni^{2+}), the protein concentration for the neo + Ni sample was fairly low, and some Ni^{2+} apparently remained after three cycles of desalting. On the basis of the Cu and Zn contents of the sample (0.2 Cu and no Zn) and the spin concentration (0.8 spin/mol), there must be ~ 2.80 tightly bound Ni per heterodimer.

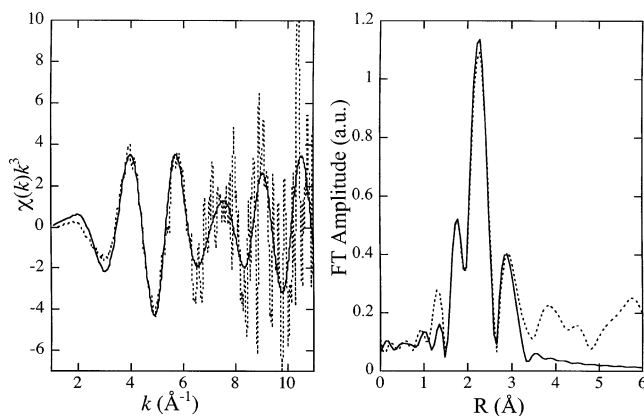


FIGURE 3: Left: $\text{Cu } k^3$ weighted EXAFS (dotted line) and its best fit (solid line) of the ophen-then-Cu-treated enzyme. Right: Fourier transform (over range $k = 1-11 \text{ \AA}^{-1}$) of the spectra described in the right panel. The best fit corresponds to fit 4 in Table 4.

Supporting Information, Table 1). These results strongly indicate that neo removes the Cu, allowing reconstitution with Ni, since, theoretically, replacement of 0.4 Cu with Ni should lead to a 66% increase in activity. To assess the effect of chelation and metal addition on ACS in the cell extract, we performed Western analysis to directly quantify the concentration of CODH/ACS, permitting measurement of the spins per mole and specific activity of ACS in the extract and at each stage in purification (Table 3). Since there is no loss of NiFeC signal intensity during the purification protocol (Table 3 and see below), it appears that the metal content is established at the time the cells are harvested and is maintained unless strong chelators are used to remove them. When the purified protein from this preparation (containing 0.4 Cu per heterodimer) was treated with neo followed by Ni^{2+} , the NiFeC signal doubled and the acetyl-CoA synthesis activity increased by 50%, which is also consistent with removal of Cu^{1+} by neo and incorporation of Ni^{2+} (22).

Therefore, neo appears to facilitate repair of CuNi forms of ACS without affecting the NiNi enzyme. ophen plays a related role of facilitating Ni removal by chelation without interacting with Cu. These observations are also consistent with the selectivity of neo for Cu^{1+} ($\beta_2 = \log K_1 + \log K_2 = 19.0$) over Ni^{2+} ($\beta_2 = 8.5$), and of ophen for Ni^{2+} ($\beta_3 = 24.0$) over Cu^{1+} ($\beta_2 = 15.8$).

The results described above support the conclusion that the CuNi enzyme is inactive and the NiNi is active. To further address whether the added Cu^{1+} is incorporated into the M_p site in the A-cluster, as observed in the crystal structure of the native enzyme, we treated CODH/ACS (containing 2.8 Ni/mol) first with ophen, then with Cu^{1+} , and finally with Ni^{2+} , with desalting carried out after each step. Neither of these two additions resulted in increase in synthesis and CoA exchange activities nor in reappearance of the original NiFeC signal observed for purified protein upon CO treatment. However, activity is markedly increased when Ni^{2+} is added to the ophen-treated purified protein (Table 1), and addition of Cu^{1+} to this sample does not significantly decrease activity. These results indicate that incorporation of Cu^{1+} into the M_p site blocks access of Ni and that incorporation of Ni^{2+} into the same site blocks access of Cu^{1+} . These results are in concurrence with those obtained using ophen- or neo-treated cell-free extracts.

Table 3: Purification of CODH/ACS^a

	protein yield (g)	CO oxidation (units)	specific activity, CO oxidation (units/mg)	NiFeC signal ($\mu\text{mol}/\text{spin}$)	amount of CODH/ACS (μmol) (antibody)	NiFeC spins/CODH/ACS heterodimer	CoA/acetyl-CoA exchange (units)
cell-free extract	13.0	178000	13.7	1.8 ± 0.2	nd	0.67 ± 0.07	325
	16.9	170000	10.1	1.1 ± 0.1	2.1 ± 0.4	0.5 ± 0.1	630 ± 30
DEAE-cellulose	4.78	188000	39	1.7 ± 0.2	nd	0.60 ± 0.06	282 ± 40
	4.26	152000	36	1.8 ± 0.2	2.8 ± 0.6	0.6 ± 0.1	360 ± 40
Q-Sepharose	1.96	172000	88	1.8 ± 0.2	nd	0.74 ± 0.07	272 ± 30
	1.05	144000	137	1.6 ± 0.2	2.2 ± 0.4	0.75 ± 0.15	700 ± 200
phenyl-Sepharose	0.495	168000	339	1.9 ± 0.1	nd	0.71 ± 0.07	720 ± 50
	0.438	153000	349	1.4 ± 0.1	2.8 ± 0.6	0.5 ± 0.1	850 ± 50
Bio-Gel A-0.5	0.270	117000	433	1.43 ± 0.05	nd	0.81 ± 0.04	690 ± 90
	0.344	153000	445	1.3 ± 0.1	2.2 ± 0.1	0.59 ± 0.03	640 ± 30

^a The data are from two independent preparations of CODH/ACS. In the second preparation, we also determined the amount of CODH/ACS by immunological methods.

Table 4: EXAFS Studies of Cu-Reconstituted CODH/ACS^a

fit	<i>N</i>	<i>R</i> (Å)	<i>s</i> ² ($\times 10^3$ Å ²)	<i>F</i> ($\times 10^3$)
1	3 S	2.328(9)	8.08	2.82
2	3 S	2.346(8)	8.18	2.57
	1 Ni/Cu	2.815(10)	6.63	
3	3 S	2.321(7)	6.92	2.43
	1 N	1.950(14)	2.00	
4	1 Ni/Cu	2.784(10)	7.99	2.41
	2.5 S	2.321(8)	5.16	
	1.18 N	1.960(20)	2.00	
	1 Ni/Cu	2.779(14)	8.50	

^a The *k* range in fit is from 1.0 to 11.0 Å⁻¹.

One of the major problems associated with studies of CODH/ACS is the heterogeneity. This is conveniently measured by the spin intensity of the NiFeC EPR signal. A completely homogeneous preparation should yield 1.0 spin per heterodimer; however, the highest fractional spin concentration of the NiFeC signal that we had observed over the past 10 years was 0.5 spin/mol (in one particular preparation). Routinely, this value has been ca. 0.2–0.4 spin/mol. On the basis of the above experiments with neo, we developed two protocols, described in Materials and Methods, that produce nearly homogeneous samples of ACS (Table 3). This involves treatment of cell-free extracts or purified enzyme with neo and then with Ni. The protocols were based on the hypothesis that, if neo can convert the CuNi into the NiNi enzyme and only the NiNi enzyme is active, one should be able to routinely repair ACS by treating cell extracts or pure protein with neo and Ni. Following the protocols outlined in Materials and Methods, we have been successful in generating samples of CODH/ACS with greatly enhanced ACS activity and NiFeC signal intensity compared with previous samples (Table 3). For example, our three most recent enzyme preparations in which the cell extracts had been treated with neo had significantly higher ACS activities (340, 230, and 275 milliunits/mg) and spin concentrations (0.8, 0.8, and 0.7 spin/mol of heterodimeric unit) than had been achieved before (see Supporting Information, Table 2). Therefore, the heterogeneity that has plagued studies of ACS for so many years seems to be explained by the metal content at the proximal metal site, and the protocol described here appears to provide a remedy for this problem.

Multifrequency EPR Studies. To investigate whether the NiFeC EPR signal of ACS arises from an $S = 1/2$ system (i.e., with spin predominantly on Ni¹⁺) or from a coupled

biradical-type system (i.e., two $S = 1/2$ systems experiencing strong electron–electron exchange and/or dipolar interactions), we performed multifrequency EPR studies. $S > 1/2$ systems may exhibit field-dependent “effective” g' -values if the electron–electron interactions are on the order of the microwave EPR frequency, while the g -values of an $S = 1/2$ system are field independent. EPR spectra were collected at S- (3.4 GHz), X- (9.19 GHz), Q- (35.0 GHz), and D- (130.0 GHz) bands. The line width (in units of magnetic field) of both the $g = 2.07$ and 2.028 peaks increases as the frequency increases due to contributions from slight inequivalence of the two highest principal g -values and/or field-dependent g -strain, with line widths for the S-shaped feature at the $g = 2.07$ peak of 12, 22, 71, and 253 G at the S-, X-, Q-, and D-bands, respectively. Similarly, the full widths at half-height for the negative absorption feature at $g = 2.03$ are 6.3, 9.6, 21, and 71 G at the S-, X-, Q-, and D-bands, respectively. To focus attention on the (in)dependence of the g -value on field/frequency, the spectra were plotted as a function of the g -value (Figure 2). The field dependence of the position of the spectral features is that expected for a species with an anisotropic g -tensor: the g -values of 2.07 and 2.03 (23) appear invariant within experimental error (± 0.003). These results indicate that the position of the spectral features arises from the field-dependent Zeeman interaction (gauged by g -values), as would be expected for an $S = 1/2$ species or a high-spin system in which the magnitude of the electron–electron interaction is much greater than the microwave frequency. As discussed below, previous EPR and ENDOR results combined with recent theoretical work suggest that the spin density is delocalized from the $S = 1/2$ Ni¹⁺ onto the $S = 0$ [4Fe4S]²⁺ center for a total $S = 1/2$ species. The electronic structure of the active site is discussed in more detail below.

Study of Cu Content in Cells, in Different Growth Media, and during Enzyme Purification. In summary, the results described above strongly indicate that the NiNi enzyme is active and the CuNi enzyme is inactive. However, the frequent association of Cu with CODH/ACS raises the obvious question: how is the Cu introduced into the protein: during purification or during cell growth? One way to address this question is to determine if the NiFeC signal and activity decrease during purification. We determined the amount (nanomoles) of CODH/ACS at each step by Western blotting, the amount of spins by EPR spectroscopy, and the

activity by methods described above at each step during purification (Table 3). If Cu is introduced during purification, the number of spins per enzyme as well as the ACS activity should decrease. However, this ratio is constant, indicating that the amount of active NiNi enzyme does not change during purification. In the second preparation shown in Table 3 (yielding 0.59 spin/mol), the stoichiometries of Cu and Ni are 0.4 and 2.6 mol/mol in the final sample of purified enzyme, indicating that the CuNi and NiNi enzymes make up 40% and 60%, respectively, of the total CODH/ACS present after the cells are lysed, which is consistent with the ratio of inactive and active protein (again demonstrating that the CuNi enzyme is inactive and the NiNi is active). These results demonstrate that Cu is not introduced into the proximal site during purification of the enzyme and suggest that Cu is introduced during cell growth. An alternative possibility is that Cu is introduced when the cells are lysed. This could occur if the Cu and CODH/ACS are located in separate cellular compartments from which Cu is released after cell lysis.

We also addressed this question of when Cu is introduced by measuring, using plasma emission spectroscopy, the Cu and Ni concentrations in the *M. thermoacetica* synthetic growth medium, in natural growth media for *M. thermoacetica* (in its ecological niche or environment), and in the buffers used during cell lysis and purification. We also measured the total intracellular Cu and Ni contents in *M. thermoacetica* cells. The buffer solutions used during cell lysis and enzyme purification were concentrated by lyophilization, subjected to plasma emission analysis, and found to lack detectable levels of Cu. This is consistent with the results described above indicating that Cu is not introduced during purification of CODH/ACS.

The standard synthetic growth medium for *M. thermoacetica* in which Cu is not supplemented was found to contain $<0.4 \mu\text{M}$ Cu and $13 \mu\text{M}$ Ni. Surprisingly, however, the intracellular concentrations in *M. thermoacetica* are $34 \mu\text{M}$ Cu and $126 \mu\text{M}$ Ni, indicating that this organism concentrates Cu at least ~ 85 -fold. This total intracellular Cu content is similar to that found in yeast, which is $200 \mu\text{M}$ (24). Since *M. thermoacetica* was first isolated from manure and anaerobic microbes that use the Wood-Ljungdahl pathway are common constituents of the GI tracts of animals and the rumen of ruminants, we measured the metal content of ruminal fluid. This natural growth medium was found to contain Cu, Ni, Fe, and Zn at the following total levels: 3, 1.5, 7.7, and $3.8 \mu\text{M}$; i.e., the Cu content is 2-fold higher than that of Ni. However, the Cu content of the ruminal fluid varies with the diet, with a recommended level of 10 ppm in beef cattle diets; for example, alfalfa hay contains 7 ppm Cu, while ryegrass and clover contain approximately 10 ppm Cu (25).

The above results indicate that there is sufficient Cu in the growing cells to supply the A-cluster with this ion and that Cu is not introduced during purification of the enzyme, although it does not prove that the Cu is not introduced during cell lysis. This issue is discussed below.

DISCUSSION

Which Form of ACS Is Active: CuNi or NiNi? The experiments described here provide unambiguous evidence

that the NiNi form of ACS is active and that the CuNi form is not. Multiple activities of ACS were measured: the intensity of the NiFeC EPR signal that is associated with the active form of ACS; acetyl-CoA synthesis from the methylated CFeSP, CO, and CoA; an exchange reaction between dephospho-CoA and acetyl-CoA that measures the ability of the enzyme to cleave and resynthesize the high-energy C-S thioester bond of acetyl-CoA; and an isotope exchange reaction between CO and acetyl-CoA that measures the ability to cleave and resynthesize the C-C and C-S bonds of acetyl-CoA. When these activities are measured on enzyme preparations containing a wide range of Cu (0.2–1.1 Cu/mol) and Ni (1.6–2.8) contents, there is a strong negative correlation between Cu content and activity that contrasts with a strong positive correlation between ACS activity and Ni content. The slope of the Ni versus activity plot is 0.5, indicating that 2 Ni are required for ACS activity, which is consistent with the need for a binuclear NiNi center at the active site of ACS. The correlation between activity and Cu content that was observed earlier (6) is restricted to samples in which the Ni concentration was constant at 2.0 Ni/mol of protein. We do not have an adequate explanation for this, but that positive correlation disappears within the broader range of Cu (0.2–1.1 Cu/mol) and Ni (1.6–2.8) contents. Perhaps the elevated Cu was related to increased levels of NiNi in the ACS active site. Moreover, those samples also show a positive correlation of CO exchange activity with Ni content (Figure 1). Since Cu^{1+} does not inhibit ACS activity (Tables 1 and 2), i.e., it only fails to support activity, a concomitant increase in Ni and Cu at the labile site of the A-cluster will appear to show a correlation of activity with Cu content.

The use of metal chelators provides further strong evidence that the A-cluster containing a CuNi site is inactive and that the NiNi form is active. Treatment of CODH/ACS, either in the purified state or in cell extracts, with ophen removes labile Ni from the A-cluster and inactivates ACS (10). When Cu^{1+} is added, none of the activities (NiFeC EPR signal, acetyl-CoA synthesis, acetyl exchange, and CO/acetyl-CoA exchange) that are lost upon ophen treatment are recovered, while addition of Ni leads to significant restoration of all these activities. It is interesting that even the least demanding activity, exchange of the acetyl group between CoA and dephospho-CoA, is not recovered by Cu^{1+} addition, especially since the CuNi enzyme can bind seleno-CoA (6). This observation may be related to the poor nucleophilicity and Lewis acidity of Cu^{1+} , which has a closed-shell d^{10} configuration. Cu-EXAFS analysis of the ophen- and Cu-treated enzyme demonstrates that the Cu is present at the proximal metal site of the A-cluster, since Cu is surrounded by three sulfurs and has the correct Cu-Ni bond distance observed in the native CuNi state of ACS, studied earlier (6). Thus, it is clear that the inactivity of the Cu^{1+} enzyme is not due to a nonspecific inactivation of the enzyme but arises from impotence of Cu^{1+} in the proximal site of the A-cluster, presumably toward nucleophilic attack on the methylated CFeSP substrate. Furthermore, addition of Ni to the ophen- and Cu-treated enzyme does not lead to recovery of activity, indicating that Cu^{1+} blocks the incorporation of Ni into the proximal site of the A-cluster. Correspondingly, addition of Cu^{1+} to the ophen- and Ni-treated enzyme does not lead to loss of activity, indicating that Ni blocks incorporation of

Cu¹⁺. Similar results were obtained with neo, which selectively removes Cu, allowing Ni to be incorporated, thus generating active enzyme. Again, Ni blocks Cu¹⁺ incorporation and Cu¹⁺ blocks reconstitution with Ni. It is important that the above treatments are performed with Cu¹⁺, since Cu²⁺ is incorporated into over 10 sites in the enzyme (9) and, as shown here, inactivates both ACS and CODH.

Development of a Protocol To Prepare Highly Active ACS. The metal replacement studies with ophen and neo suggested that a homogeneous NiNi enzyme could be obtained by replacing the Cu at the proximal metal site with Ni. This prediction was realized by treating cell extracts or purified protein with neo, which selectively removes Cu¹⁺, followed by Ni, which can then bind to the proximal center. These procedures allow the generation of nearly homogeneous NiNi CODH/ACS, i.e., 80% in the active NiNi state. The heterogeneity that has plagued studies of ACS for so many years seems to be explained by the metal content at the proximal metal site, and the protocol described here appears to provide a partial remedy for this problem. Preparations of CODH/ACS still contain some Zn (which, like Cu, does not support activity) at the proximal site, so a challenge still remains to replace the Zn with Ni, which we predict will yield completely homogeneous and fully active ACS.

Which Form of ACS Elicits the NiFeC EPR Signal and What Is the Electronic Structure of the A-Cluster? The spin concentration of the so-called NiFeC EPR signal closely tracks activity (6), consistent with the hypothesis that it is a catalytically competent intermediate in the reaction mechanism of ACS (1, 26), though this has been disputed (27). Recent DFT calculations addressed two models of the electronic state of the NiFeC species: model 1 including a [4Fe-4S]²⁺ cluster linked to Ni¹⁺ at the M_p site, which is bridged to a Ni²⁺ at the M_d site, and model 2, which is similar except that Cu¹⁺ is at the M_p site and Ni¹⁺ is located at the distal site. In both of these models, the spin resides predominantly on the Ni¹⁺, which has an electronic spin, $S = 1/2$, since the other components of the A-cluster have net spins, $S = 0$. The calculations (28) support model 1; however, there is another possible model (6), model 3, that was not addressed by the DFT calculations in which the EPR signal derives from the CuNi enzyme in a state that consists of a reduced [4Fe-4S]¹⁺ cluster and the distal Ni¹⁺. Cu¹⁺ would harbor an insignificant fraction of the electronic spin, in accordance with DFT calculations (28), effectively insulating the two $S = 1/2$ species from through-bond exchange interactions. However, strong dipolar interactions may still occur because the FeS cluster and the distal Ni are very close, similar to the radical doublet observed in some adenosylcobalamin-dependent enzymes (29, 30): if the magnitude of the electron–electron dipolar interactions were on the order of the microwave frequency, spectral features may exhibit field- and frequency-dependent effective g' -values. However, the multifrequency EPR studies described here demonstrate that the g -values remain the same over a large range in frequencies (3–130 GHz), indicating that the NiFeC signal is either an $S = 1/2$ species or a high-spin species with an electron–electron interaction significantly greater than 130 GHz in magnitude. Recent theoretical and Mössbauer work (28) as well as preliminary EPR relaxation measurements strongly suggests that the NiFeC signal does not arise from a high-spin (diradical) species but from an $S = 1/2$

system. This result is in clear conflict with model 3 and is consistent with model 1. Thus, it appears that the NiFeC EPR signal can arise only from the NiNi form of the enzyme and that the electronic structure of this paramagnetic species consists of a diamagnetic [4Fe-4S]²⁺ cluster linked to the proximal Ni¹⁺ ion, which carries most of the $S = 1/2$ spin. The unpaired spin density on the proximal Ni¹⁺ was calculated to be about 43% of the total spin density and about 20% of the total spin density delocalized onto the [4Fe-4S]²⁺ cluster, through being strongly coupled ($J = 100–120 \text{ cm}^{-1}$) to an $S = 5/2$ Fe(III) atom in the cluster, thus generating the nonzero ⁵⁷Fe hyperfine interactions observed by Mössbauer, ENDOR, and EPR spectroscopy (28). The distal Ni, which is in a planar four-coordinate environment with two deprotonated amides, is viewed to be a low-spin ($S = 0$) Ni²⁺ state, without any appreciable spin density. This view would be consistent with prior Mössbauer data that provided evidence that the NiFeC species contains a [4Fe-4S]²⁺ cluster (31, 32).

Besides illustrating the relative field independence of the spectral g -values, Figure 2 also demonstrates that the two predominant spectral features at $g = 2.07$ and 2.03 are affected differently by separate line-broadening mechanisms. In this plot, which uses g -values as the independent variable, the $g = 2.07$ peak is approximately field/frequency independent (at X-band and above) as would be expected for a peak dominated by a field-dependent broadening mechanism such as unresolved, inequivalent g -values and/or g -strain. However, the $g = 2.03$ peak becomes consistently narrower as the field/frequency increases, indicating that its width is dominated by field-independent interactions such as unresolved electron–nuclear hyperfine interactions (33, 34) or electron–electron exchange/dipolar interactions. Nuclei in this system that could elicit hyperfine broadening are Cu ($I = 3/2$), N ($I = 1$), and H ($I = 1/2$). We have been unable to detect hyperfine structure from the Cu¹⁺ ion by EPR, ESEEM, or ENDOR spectroscopy (Ragsdale and Britt, unpublished results). The Ni center at M_p is sulfur-rich, containing three cysteine ligands, so it is feasible that the β protons of the cysteine ligands are the source of the broadening. There are no nitrogen ($I = 1$) ligands to the proximal Ni, ruling this out as a contributor to hyperfine structure. Other contributions to line broadening are dipole–dipole interactions and exchange broadening, which may arise from the significant spin density from the proximal Ni¹⁺ that is delocalized onto the [4Fe-4S]²⁺ cluster, through a bridging cysteine ligand (see above).

Origin of the Cu in the M_p Site. As described above, the vulnerability of the proximal metal site in the A-cluster to substitution with different metals appears to be responsible for the heterogeneity that has plagued studies of CODH/ACS for so many years. However, it raises the question: when is Cu (or Zn) introduced into the protein? One possibility is that only the NiNi protein is present in living cells and Cu or Zn replaces the Ni at the M_p site either when the cells are lysed or during purification of the enzyme. The other possibility is that Cu, Zn, and Ni are incorporated into the protein during growth so that varying amounts of the NiNi, CuNi, and ZnNi enzymes are present in growing cells. The latter scenario is less attractive since it would appear to be counterproductive for cells to allow the key enzyme in anaerobic CO₂ fixation by the Wood–Ljungdahl pathway

to be so nonselective as to incorporate metals (Cu and Zn) that do not support activity.

We addressed this question by measuring the Cu and Ni concentrations in the *M. thermoacetica* synthetic growth medium, in natural growth media for *M. thermoacetica* (in its ecological niche or environment), and in the buffers used during cell lysis and purification. We also measured the total intracellular Cu and Ni contents within *M. thermoacetica* cells. Based strictly on where Cu is most abundant, the results indicate that the Cu is introduced during cell growth since Cu is in much higher total concentration within growing cells than in the solutions that the enzyme is exposed to during purification. In fact, cells of *M. thermoacetica* concentrate Cu over 85-fold and Ni at least 10-fold from the growth medium. The Cu importer CopA has been located in all kingdoms of life, including the anaerobic microbe *Archaeoglobus fulgidus*, from which it has been characterized (35) along with CopB, which is another P-type Cu-transporting ATPase, and a putative Atx1- or CopZ-type Cu chaperone. Another potential protein involved in the import of Ni and Cu is NikA, which binds Ni with a $K_d < 0.1 \mu\text{M}$ and divalent Co, Cu, and Fe with at least 10-fold lower affinity (36). Whether these Cu metabolizing proteins are present in *M. thermoacetica* awaits the impending determination of the *M. thermoacetica* genome sequence.

The above results indicate that there is sufficient Cu in growing cells to supply the A-cluster with this ion. However, although total intracellular Cu is present at fairly high concentrations, free Cu (and Zn) is present at very low levels in cells: less than one atom per *Escherichia coli* cell (37, 38). A consensus seems to be developing that all the metal-dependent proteins in the cell are involved in exquisite trafficking pathways and interact selectively with specific chaperones that deliver the metal to the active site. Cu (39) and Ni (40) metallochaperones have been characterized, including a potential Ni chaperone for CODH/ACS (41). Thus, one might argue that, since the CuNi enzyme is inactive and the NiNi enzyme is active, Ni-specific metallochaperones insert this metal into ACS, and the presence of Cu in the enzyme results from its introduction during cell lysis. This could occur if the Cu and CODH/ACS are sequestered within separate compartments within the cell and Cu is released after lysis. However, the amount of ACS activity (and thus NiNi enzyme) is determined by the state of the cells at the time of lysis, and this value does not change during purification, which suggests that Cu is introduced into the proximal site in the A-cluster during growth of the cells. Furthermore, even in the presence of elevated levels of high-affinity chelators, exchange of Cu for Ni (or Ni for Cu) at the M_p site in cell extracts or in the purified protein occurs very slowly. Further studies are clearly warranted to explore these alternative possibilities.

If Cu is introduced during cell growth, one might speculate that incorporation of Cu could serve to protect against inactivation, to play a role as an intermediate in assembly of the NiNi center, to play a regulatory role, or to promote an alternative activity. There are examples of enzymes in which several metals support activity (42, 43). One of the most interesting examples is with a dioxygenase involved in the methionine salvage pathway that can bind different metal ions, which confers different product distributions; for example, the Ni enzyme generates CO, but the Fe enzyme

produces formate (44). Furthermore, the metallochaperone UreE can bind Cu or Ni (42), and methionine aminopeptidase can bind Mn, Co, and Zn, though recent evidence indicates this is a Mn enzyme (45). In recent results that support a beneficial or protective role for Cu, it was found that when Cu was removed from the growth medium and from all buffers during purification by chelation with neo, the purified ACS contained 0.05 Cu and no ACS activity; furthermore, treatment with Ni only led to recovery of 50% of the ACS activity (9). In that study neo appeared to have chelated both Cu and Ni from the labile site, whereas the present results indicate neo chelation of Cu only. Further studies will be required to explore whether there is any role for the CuNi form of ACS. Before the structure of CODH/ACS was revealed, Cu had never before been detected as a component of an enzyme from a strict anaerobe; it is usually associated with oxygen-based chemistry. The Cu-containing nitrous oxide reductase from denitrifying bacteria could be cited, but these organisms inhabit the oxic/anoxic interface (46, 47). This enzyme contains a tetranuclear Cu cluster and a binuclear Cu center (48, 49).

CONCLUSION

Results described here indicate that the NiNi form of ACS is active, while the CuNi form is not. It appears that the heterogeneity that has compromised interpretations of kinetic and spectroscopic data on ACS results from the heterogeneous metal composition at the proximal metal center of the A-cluster in ACS. A metal replacement protocol has been developed that allows the generation of nearly homogeneous NiNi enzyme with high activity and intensity of the NiFeC EPR signal. The Cu appears to be incorporated into the enzyme either during cell growth or between the time that cells are lysed and enzyme purification begins.

ACKNOWLEDGMENT

We thank Elizabeth Pierce for help in purifying the samples of CODH/ACS used in these studies. Use of the Advanced Photon Source was supported by the U.S. Department of Energy, Basic Energy Sciences, Office of Science, under Contract W-31-109-ENG-38. BioCAT is a National Institutes of Health-supported Research Center (RR-08630).

SUPPORTING INFORMATION AVAILABLE

Two tables giving results for cell-free extracts from *Moorella* cells grown with $4 \mu\text{M}$ Cu and $20 \mu\text{M}$ Ni in growth media and properties of CODH/ACS purified with acid-washed glassware. This material is available free of charge via the Internet at <http://pubs.acs.org>.

REFERENCES

1. Ragsdale, S. W. (2000) Nickel Containing CO Dehydrogenases and Hydrogenases, in *Enzyme-Catalyzed Electron and Radical Transfer* (Holzenburg, A., and Scrutton, N., Eds.) pp 487–518, Plenum Press, New York.
2. Ragsdale, S. W., and Kumar, M. (1996) Ni containing carbon monoxide dehydrogenase/acetyl-CoA synthase, *Chem. Rev.* 96, 2515–2539.
3. Ragsdale, S. W. (1999) The Acetogenic Corrinoid Proteins, in *Chemistry and Biochemistry of B₁₂* (Banerjee, R., Ed.) pp 633–654, John Wiley and Sons, New York.

4. Doukov, T. I., Iverson, T., Seravalli, J., Ragsdale, S. W., and Drennan, C. L. (2002) A Ni-Fe-Cu center in a bifunctional carbon monoxide dehydrogenase/acetyl-CoA synthase, *Science* 298, 567–572.
5. Darnault, C., Volbeda, A., Kim, E. J., Legrand, P., Vernede, X., Lindahl, P. A., and Fontecilla-Camps, J. C. (2003) Ni-Zn-[Fe(4)-S(4)] and Ni-Ni-[Fe(4)-S(4)] clusters in closed and open alpha subunits of acetyl-CoA synthase/carbon monoxide dehydrogenase, *Nat. Struct. Biol.* 10, 271–279.
6. Seravalli, J., Gu, W., Tam, A., Strauss, E., Begley, T. P., Cramer, S. P., and Ragsdale, S. W. (2003) Functional copper at the acetyl-CoA synthase active site, *Proc. Natl. Acad. Sci. U.S.A.* 100, 3689–3694.
7. Hausinger, R. P. (2003) Ni and CO: more surprises, *Nat. Struct. Biol.* 10, 234–236.
8. Gencic, S., and Grahame, D. A. (2003) Nickel in subunit beta of the acetyl-CoA decarbonylase/synthase multienzyme complex in methanogens: Catalytic properties and evidence for a binuclear Ni–Ni site, *J. Biol. Chem.* 278, 6101–6110.
9. Bramlett, M. R., Tan, X., and Lindahl, P. A. (2003) Inactivation of Acetyl-CoA Synthase/Carbon Monoxide Dehydrogenase by Copper, *J. Am. Chem. Soc.* 125, 9316–9317.
10. Shin, W., and Lindahl, P. A. (1992) Function and CO binding properties of the NiFe complex in carbon monoxide dehydrogenase from *Clostridium thermoaceticum*, *Biochemistry* 31, 12870–12875.
11. Russell, W. K., Stalhandske, C. M. V., Xia, J. Q., Scott, R. A., and Lindahl, P. A. (1998) Spectroscopic, redox, and structural characterization of the Ni-labile and nonlabile forms of the acetyl-CoA synthase active site of carbon monoxide dehydrogenase, *J. Am. Chem. Soc.* 120, 7502–7510.
12. Lundie, L. L., Jr., and Drake, H. L. (1984) Development of a minimally defined medium for the acetogen *Clostridium thermoaceticum*, *J. Bacteriol.* 159, 700–703.
13. Ragsdale, S. W., Clark, J. E., Ljungdahl, L. G., Lundie, L. L., and Drake, H. L. (1983) Properties of purified carbon monoxide dehydrogenase from *Clostridium thermoaceticum* a nickel, iron-sulfur protein, *J. Biol. Chem.* 258, 2364–2369.
14. Bhaskar, B., DeMoll, E., and Grahame, D. A. (1998) Redox-dependent acetyl transfer partial reaction of the acetyl-CoA Decarbonylase/Synthase complex: kinetics and mechanism, *Biochemistry* 37, 14491–14499.
15. Seravalli, J., and Ragsdale, S. W. (2000) Channeling of Carbon Monoxide during Anaerobic Carbon Dioxide Fixation, *Biochemistry* 39, 1274–1277.
16. Maynard, E. L., Sewell, C., and Lindahl, P. A. (2001) Kinetic mechanism of acetyl-coa synthase: steady-state synthesis at variable co/co(2) pressures, *J. Am. Chem. Soc.* 123, 4697–4703.
17. Elliott, J. L., and Brewer, J. M. (1978) The inactivation of yeast enolase by 2,3-butanedione, *Arch. Biochem. Biophys.* 190, 351–357.
18. Froncisz, W., and Hyde, J. S. (1982) The Loop-Gap Resonator: A New Microwave Lumped Circuit ESR Sample Structure, *J. Magn. Reson.* 47, 515.
19. Hyde, J. S., Newton, M. E., Strangeway, R. A., Camenisch, T. G., and Froncisz, W. (1991) Electron Paramagnetic Resonance Q-band Bridge with GaAs Field-Effect Transistor Signal Amplifier and Low-Noise Gunn Diode Oscillator, *Rev. Sci. Instrum.* 62, 2969–2975.
20. Dorlet, P., Seibold, S. A., Babcock, G. T., Gerfen, G. J., Smith, W. L., Tsai, A., and Un, S. (2002) High-Field EPR Study of the Tyrosyl Radicals in Prostaglandin H2 Synthase-1, *Biochemistry* 41, 6107–6114.
21. Shin, W., Anderson, M. E., and Lindahl, P. A. (1993) Heterogeneous nickel environments in carbon monoxide dehydrogenase from *Clostridium thermoaceticum*, *J. Am. Chem. Soc.* 115, 5522–5526.
22. Martell, A. E., and Smith, R. M. (1975) *Critical Stability Constants*, Vol. 2, Plenum Publishing Co., New York.
23. Ragsdale, S. W., Wood, H. G., and Antholine, W. E. (1985) Evidence that an iron-nickel-carbon complex is formed by reaction of CO with the CO dehydrogenase from *Clostridium thermoaceticum*, *Proc. Natl. Acad. Sci. U.S.A.* 82, 6811–6814.
24. Rae, T. D., Schmidt, P. J., Pufahl, R. A., Culotta, V. C., and O'Halloran, T. V. (1999) Undetectable intracellular free copper: the requirement of a copper chaperone for superoxide dismutase, *Science* 284, 805–808.
25. Grace, N. (1975) Studies on the flow of zinc, cobalt, copper, and manganese along the digestive tract of sheep given fresh perennial ryegrass, or white or red clover, *Br. J. Nutr.* 34, 73–82.
26. Seravalli, J., Kumar, M., and Ragsdale, S. W. (2002) Rapid Kinetic Studies of Acetyl-CoA Synthase: Evidence Supporting the Catalytic Intermediacy of a Paramagnetic NiFeC Species in the Autotrophic Wood-Ljungdahl Pathway, *Biochemistry* 41, 1807–1819.
27. Lindahl, P. A. (2002) The Ni-containing carbon monoxide dehydrogenase family: light at the end of the tunnel?, *Biochemistry* 41, 2097–2105.
28. Schenker, R. P., and Brunold, T. C. (2003) Computational studies on the A cluster of acetyl-coenzyme A synthase: geometric and electronic properties of the NiFeC species and mechanistic implications, *J. Am. Chem. Soc.* 125, 13962–13963.
29. Banerjee, R., and Ragsdale, S. W. (2003) The Many Faces of Vitamin B₁₂: Catalysis by Cobalamin-dependent Enzymes, *Annu. Rev. Biochem.* 72, 209–247.
30. Licht, S., Gerfen, G. J., and Stubbe, J. A. (1996) Thiyl radicals in ribonucleotide reductases, *Science* 271, 477–481.
31. Xia, J. Q., Hu, Z. G., Popescu, C. V., Lindahl, P. A., and Munck, E. (1997) Mossbauer and EPR study of the Ni-activated alpha-subunit of carbon monoxide dehydrogenase from *Clostridium thermoaceticum*, *J. Am. Chem. Soc.* 119, 8301–8312.
32. Lindahl, P. A., Ragsdale, S. W., and Münck, E. (1990) Mössbauer studies of CO dehydrogenase from *Clostridium thermoaceticum*, *J. Biol. Chem.* 265, 3880–3888.
33. Pierik, A. J., Hagen, W. R., Dunham, W. R., and Sands, R. H. (1992) Multi-frequency EPR and high-resolution Mossbauer spectroscopy of a putative [6Fe-6S] prismatic-cluster-containing protein from *Desulfovibrio vulgaris* (Hildenborough). Characterization of a supercluster and superspin model protein, *Eur. J. Biochem.* 206, 705–719.
34. Hagen, W. R., and Albracht, S. P. (1982) Analysis of strain-induced EPR-line shapes and anisotropic spin-lattice relaxation in a [2Fe-2S] ferredoxin, *Biochim. Biophys. Acta* 702, 61–71.
35. Mandal, A. K., Cheung, W. D., and Arguello, J. M. (2002) Characterization of a thermophilic P-type Ag⁺/Cu⁺-ATPase from the extremophile *Archaeoglobus fulgidus*, *J. Biol. Chem.* 277, 7201–7208.
36. De Pina, K., Navarro, C., McWalter, L., Boxer, D. H., Price, N. C., Kelly, S. M., Mandrandberthelot, M. A., and Wu, L. F. (1995) Purification and characterization of the periplasmic nickel-binding protein NikA of *Escherichia coli* K12, *Eur. J. Biochem.* 227, 857–865.
37. Outten, C. E., and O'Halloran, T. V. (2001) Femtomolar sensitivity of metalloregulatory proteins controlling zinc homeostasis, *Science* 292, 2488–2492.
38. Changela, A., Chen, K., Xue, Y., Holschen, J., Outten, C. E., O'Halloran, T. V., and Mondragon, A. (2003) Molecular basis of metal-ion selectivity and zeptomolar sensitivity by CueR, *Science* 301, 1383–1387.
39. Rosenzweig, A. C. (2001) Copper delivery by metallochaperone proteins, *Acc. Chem. Res.* 34, 119–128.
40. Mulrooney, S. B., and Hausinger, R. P. (2003) Nickel uptake and utilization by microorganisms, *FEMS Microbiol. Rev.* 27, 239–261.
41. Loke, H. K., and Lindahl, P. A. (2003) Identification and preliminary characterization of AcsF, a putative Ni-insertase used in the biosynthesis of acetyl-CoA synthase from *Clostridium thermoaceticum*, *J. Inorg. Biochem.* 93, 33–40.
42. Song, H. K., Mulrooney, S. B., Huber, R., and Hausinger, R. P. (2001) Crystal structure of *Klebsiella aerogenes* UreE, a nickel-binding metallochaperone for urease activation, *J. Biol. Chem.* 276, 49359–49364.
43. Kishishita, S., Okajima, T., Kim, M., Yamaguchi, H., Hirota, S., Suzuki, S., Kuroda, S., Tanizawa, K., and Mure, M. (2003) Role of copper ion in bacterial copper amine oxidase: spectroscopic and crystallographic studies of metal-substituted enzymes, *J. Am. Chem. Soc.* 125, 1041–1055.
44. Dai, Y., Wensink, P. C., and Abeles, R. H. (1999) One protein, two enzymes, *J. Biol. Chem.* 274, 1193–1195.
45. Wang, J., Sheppard, G. S., Lou, P., Kawai, M., Park, C., Egan, D. A., Schneider, A., Bouska, J., Lesniowski, R., and Henkin, J. (2003) Physiologically Relevant Metal Cofactor for Methionine Aminopeptidase-2 Is Manganese, *Biochemistry* 42, 5035–5042.
46. Jetten, M. S., Strous, M., van de Pas-Schoonen, K. T., Schalk, J., van Dongen, U. G., van de Graaf, A. A., Logemann, S., Muyzer,

- G., van Loosdrecht, M. C., and Kuenen, J. G. (1998) The anaerobic oxidation of ammonium, *FEMS Microbiol. Rev.* 22, 421–437.
47. Brettar, I., Moore, E. R., and Hofle, M. G. (2001) Phylogeny and Abundance of Novel Denitrifying Bacteria Isolated from the Water Column of the Central Baltic Sea, *Microb. Ecol.* 42, 295–305.
48. Haltia, T., Brown, K., Tegoni, M., Cambillau, C., Saraste, M., Mattila, K., and Djinovic-Carugo, K. (2003) Crystal structure of nitrous oxide reductase from *Paracoccus denitrificans* at 1.6 Å resolution, *Biochem. J.* 369, 77–88.
49. Prudencio, M., Pereira, A. S., Tavares, P., Besson, S., Cabrito, I., Brown, K., Samyn, B., Devreese, B., Van Beeumen, J., Rusnak, F., Fauque, G., Moura, J. J., Tegoni, M., Cambillau, C., and Moura, I. (2000) Purification, characterization, and preliminary crystallographic study of copper-containing nitrous oxide reductase from *Pseudomonas nautica* 617, *Biochemistry* 39, 3899–3907.

BI036194N